

All-microwave CZ gate based on fixed-frequency driven coupler

Wanpeng Gao(高万鹏), Xiaoliang He(何潇梁), Zhengqi Niu(牛铮琦), Daqiang Bao(包大强), Kuang Liu(刘匡), Junfeng Chen(陈俊锋), Zhen Wang(王镇), and Z. R. Lin(林志荣)

Citation: Chin. Phys. B, 2025, 34 (**4**): 040304. DOI: 10.1088/1674-1056/adb68a
Journal homepage: http://cpb.iphy.ac.cn; http://iopscience.iop.org/cpb

What follows is a list of articles you may be interested in

Global receptive field transformer decoder method on quantum surface code data and syndrome error correction

Ao-Qing Li(李熬庆), Ce-Wen Tian(田策文), Xiao-Xuan Xu(徐晓璇), Hong-Yang Ma(马鸿洋), and Jun-Qing Liang(梁俊卿)
Chin. Phys. B, 2025, 34 (**3**): 030306. DOI: 10.1088/1674-1056/adab63

Quantum decoder design for subsystem surface code based on multi-head graph attention and edge weighting

Nai-Hua Ji(纪乃华), Hui-Qian Sun(孙汇倩), Bo Xiao(肖博), Ping-Li Song(宋平俐), and Hong-Yang Ma(马鸿洋)
Chin. Phys. B, 2025, 34 (**2**): 020309. DOI: 10.1088/1674-1056/ada1c7

Correcting on-chip distortion of control pulses with silicon spin qubits

Ming Ni(倪铭), Rong-Long Ma(马荣龙), Zhen-Zhen Kong(孔真真), Ning Chu(楚凝), Wei-Zhu Liao(廖伟筑), Sheng-Kai Zhu(祝圣凯), Chu Wang(王儲), Gang Luo(罗刚), Di Liu(刘頓), Gang Cao(曹刚), Gui-Lei Wang(王桂磊), Hai-Ou Li(李海欧), and Guo-Ping Guo(郭国平)
Chin. Phys. B, 2025, 34 (**1**): 010308. DOI: 10.1088/1674-1056/ad8db1

Coupling and characterization of a Si/SiGe triple quantum dot array with a microwave resonator

Shun-Li Jiang(江顺利), Tian-Yi Jiang(蒋天翼), Yong-Qiang Xu(徐永强), Rui Wu(吴睿), Tian-Yue Hao(郝天岳), Shu-Kun Ye(叶澍坤), Ran-Ran Cai(蔡冉冉), Bao-Chuan Wang(王保传), Hai-Ou Li(李海欧), Gang Cao(曹刚), and Guo-Ping Guo(郭国平)
Chin. Phys. B, 2024, 33 (**9**): 090311. DOI: 10.1088/1674-1056/ad711d

In-situ deposited anti-aging TiN capping layer for Nb superconducting quantum circuits

Hao-Ran Tao(陶浩然), Lei Du(杜磊), Liang-Liang Guo(郭亮亮), Yong Chen(陈勇), Hai-Feng Zhang(张海峰), Xiao-Yan Yang(杨小燕), Guo-Liang Xu(徐国良), Chi Zhang(张 驰), Zhi-Long Jia(贾志龙), Peng Duan(段鹏), and Guo-Ping Guo(郭国平)
Chin. Phys. B, 2024, 33 (**9**): 090310. DOI: 10.1088/1674-1056/ad6a3c

---

RAPID COMMUNICATION

All-microwave CZ gate based on fixed-frequency driven coupler

Wanpeng Gao(高万鹏)[1,2], Xiaoliang He(何潇梁)[1,2], Zhengqi Niu(牛铮琦)[1,3], Daqiang Bao(包大强)[1], Kuang Liu(刘匡)[1], Junfeng Chen(陈俊锋)[1,2], Zhen Wang(王镇)[1,2,3], and Z. R. Lin(林志荣)[1,2,†]

[1] *State Key Laboratory of Materials for Integrated Circuits, Shanghai Institute of Microsystem and Information Technology, Chinese Academy of Sciences, Shanghai* 200050, *China*

[2] *University of Chinese Academy of Sciences, Beijing* 100049, *China*

[3] *ShanghaiTech University, Shanghai* 201210, *China*

(Received 23 January 2025; revised manuscript received 14 February 2025; accepted manuscript online 17 February 2025)

High-quality entangling gates are crucial for scalable quantum information processing. Implementing all-microwave two-qubit gates on fixed-frequency transmons offers advantages in reducing wiring complexity, but the gate performance is often limited due to the residual *ZZ* interaction and the frequency crowding problem. Here, we introduce a novel scheme that enables a microwave drive-activated CZ gate compatible with the coupler structure to suppress the residual *ZZ* interaction. The microwave drive is applied to the coupler and the microwave drive frequency remains far detuned from the system's transition frequency to alleviate the frequency crowding problem. We model the gate process analytically and demonstrate a theoretical gate fidelity up to 99.9% numerically. Our scheme is compatible with current coupler-structure-based circuits, and insensitive to microwave crosstalk, showing a possible path for all-microwave quantum operations at scale.

Keywords: quantum computing, superconducting qubit, two-qubit gate

PACS: 03.67.Lx

DOI: 10.1088/1674-1056/adb68a **CSTR:** 32038.14.CPB.adb68a

The development of high-quality, scalable entangling gates is essential for achieving large-scale fault-tolerant quantum computing.[1–3] Superconducting circuits represent a promising approach due to their facile on-chip integration and high gate fidelity.[4–7] Fixed-frequency transmons boast high connectivity and long coherence times, and are commonly used as basic modules in superconducting quantum circuits.[8,9] Consequently, various all-microwave two-qubit gate schemes have been proposed based on fixed-frequency transmons.[10–18]

All-microwave two-qubit gates utilize microwave drives to monitor the system's evolution along a specific trajectory[15–17,19] or activate interactions between computational states by creating adjustable virtual energy states.[10–12] In most schemes, residual *ZZ* coupling between qubits induced by weak anharmonicities of transmons can cause coherent errors and decline the gate performance, and a widely adopted solution is introducing the coupler structure.[20–24] Considering all-microwave two-qubit gate schemes based on the coupler structure, an ideal scheme should allow us to apply the microwave drive on the coupler to achieve precise control and suppress microwave crosstalk in a large system.[16] Besides, the required microwave drive frequency should be far-detuned from any possible transition frequency in the system, and any higher energy levels of the transmon should be avoided during the gate process due to their poor coherence time.

In this study, we propose a novel all-microwave two-qubit gate scheme based on the coupler structure, with transverse and longitudinal coupling between data qubits suppressed by the coupler. The interaction is activated by applying a microwave pulse to the coupler with a frequency close to the frequency difference between the $|11\rangle$ state of data qubits and the coupler. This microwave pulse monitors the system's evolution along a specific trajectory, while the $|11\rangle$ state acquires a π phase during the process and enables a CZ gate.[25,26] This process can also be understood as a four-wave mixing process at single-photon level, where two photons from each data qubit convert to one photon stored in the coupler and the other propagating along with microwave drive. Crucially, the microwave drive is applied at a frequency far detuned from any direct system transitions, offering a robust solution to the pervasive issue of frequency crowding in large-scale quantum computing. This innovative approach not only mitigates frequency crowding but also enhances scalability, paving the way for more compact all-microwave quantum computing architectures.

Our scheme requires a pair of qubits coupled with a coupler, as shown in Fig. 1(a), with circuit Hamiltonian modeled as coupled Duffing oscillators

$$H/\hbar = \sum_{i=1,2,c} \omega_i a_i^\dagger a_i + \frac{\alpha}{2} a_i^\dagger a_i^\dagger a_i a_i$$

†Corresponding author. E-mail: zrlin@mail.sim.ac.cn

© 2025 Chinese Physical Society and IOP Publishing Ltd. All rights, including for text and data mining, AI training, and similar technologies, are reserved.

$$+\sum_{j=1,2} g_j(a_j^\dagger + a_j)(a_c^\dagger + a_c)$$
$$+g_{12}(a_1^\dagger + a_1)(a_2^\dagger + a_2), \quad (1)$$

where $\hbar$ is the reduced Planck constant, a_i and $a_i^\dagger$ ($i \in 1,2,c$) are the annihilation and creation operators of the i-th qubit, ω_i and α_i are the resonant frequency and anharmonicity of each qubit, g_{ic} is the transverse coupling strength between the i-th qubit and the coupler, and g_{12} is the direct transverse coupling strength between the data qubits. This Hamiltonian can be realized in a superconducting quantum circuit as shown in Fig. 1(b).

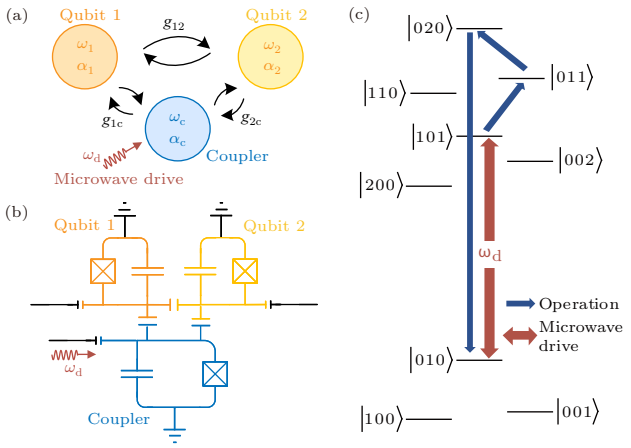


Fig. 1. Schematic and concept of the CZ gate scheme. (a) Schematic of the CZ gate scheme. The scheme requires a pair of coupled qubits (orange & yellow) and a coupler (blue), the gate is activated with a microwave drive applied to the coupler. (b) The diagram of a superconducting circuit realizing the system of a pair of coupled qubits and the coupler. (c) Energy-level diagram of the system with microwave drive. The microwave drive (red) frequency is close to the $|101\rangle \leftrightarrow |010\rangle$ transition frequency. A population exchange can take place between $|101\rangle$ and $|010\rangle$, one possible path is shown in blue arrows.

To induce the interaction between data qubits, we apply a microwave drive

$$H_d/\hbar = \Omega(a_c^\dagger e^{-i\omega_d t} + a_c e^{i\omega_d t}) \quad (2)$$

to the coupler, with amplitude Ω_d, and frequency ω_d close to the $|101\rangle \leftrightarrow |010\rangle$ transition frequency (eigenstate $|ijk\rangle$ stands for $|i\rangle_1 |j\rangle_c |k\rangle_2$). The population of state $|101\rangle$ can be transferred to state $|010\rangle$ with this microwave drive, and be transferred back acquiring a π phase in this process. Note that a similar mechanism can be used to exchange a single photon between two cavities.[27] Multiple possible paths exist for this process with different effective drive strengths, and the effective drive strength of one typical path (as shown in Fig. 1(c)) can be expressed as

$$\Omega_{path} = \frac{\sqrt{2} g_{1c} g_{2c} \Omega_d}{(\omega_d - \omega_1 - \omega_2)(\omega_2 - \omega_c - \alpha_c)}. \quad (3)$$

The total effective drive strength can be therefore calculated by adding the effective drive strength of all paths, with the total effective drive strength expressed as $\Omega_{total} = \sum_{i-\text{th path}} \Omega_{path}$. As shown in Eq. (3), Ω_{total} is proportional to the coupling strength g_{1c}, g_{2c} and the microwave drive strength Ω_d. Ω_{total} is also affected by factors related to the detuning between states involved in this Raman-like process. Nonetheless, these paths interfere destructively, resulting in a limited effective drive strength, especially when the detuning between the data qubits is larger than their anharmonicities. Baring these concerns, we choose the system parameters as the following: the frequencies of Q_1, Q_2 and coupler are $\omega_1/2\pi = 4.25$ GHz, $\omega_2/2\pi = 4.35$ GHz, and $\omega_c/2\pi = 4.75$ GHz; anharmonicities of the qubits are $\alpha_1/2\pi = -150$ MHz, $\alpha_2/2\pi = -150$ MHz, and $\alpha_c/2\pi = -210$ MHz. The transverse coupling strengths between qubits and coupler are $g_{1c}/2\pi = 100$ MHz and $g_{2c}/2\pi = 100$ MHz; the transverse coupling strength between data qubits is $g_{12}/2\pi = 23.6$ MHz. These transverse coupling strengths are set to turn off the transverse and longitudinal interaction between data qubits simultaneously.

One may notice that the system is not fully operated in the dispersive regime $|g_{ic}/\Delta_{ic}| \ll 1$, where $\Delta_{ic} = \omega_i - \omega_c$, due to the strong coupling required by fast operation. This questions the accuracy of most analytical approaches to the effective drive strength Ω_{total}. Here, we directly calculate the driven ZZ interaction ξ_{drive} caused by microwave drive Ω_{total} numerically.[28] We first consider the static ZZ interaction ξ_{static} resulting from the interaction between the state $|101\rangle$ and non-computational states, such as $|200\rangle$. Therefore, we can compare the ZZ interaction strength

$$\xi_{ZZ} = \epsilon_{101} - \epsilon_{100} - \epsilon_{001} + \epsilon_{000} \quad (4)$$

before and after introducing the interaction between the state $|101\rangle$ and non-computational states, and the difference is the static ZZ interaction ξ_{static}. Here ϵ_{ijk} is the eigenenergy of the state $|ijk\rangle$ or the eigenenergy of the eigenstate that most resembles the state $|ijk\rangle$ while we introduce the interaction. We can repeat this while adding a microwave drive to the system, with eigenstates replaced by time-dependent dressed states. We extract the difference before and after introducing the microwave drive, resulting in the driven ZZ interaction ξ_{drive}. The results are obtained with the first three energy levels of each qubit and the coupler taken into account.

Figure 2(a) displays the energy difference between time-dependent dressed states and their corresponding eigenstates without the microwave drive. We calculate the energy difference while varying the microwave drive frequency, with the microwave drive strength fixed at 200 MHz. The eigenenergies of all dressed states reachable within two excitations are shown in Fig. 2(a), with computational states plotted in bold lines. The eigenenergy fluctuation reflects population exchange with another eigenstate induced by the microwave

drive, with the transient point showing the on-resonance microwave drive frequency. The eigenenergies' fluctuations around 4.1 GHz and 4.2 GHz result from excitations of Q_1 $|1\rangle \leftrightarrow |2\rangle$ transition and Q_2 $|1\rangle \leftrightarrow |2\rangle$ transition, respectively. The tiny fluctuation around 3.77 GHz (marked in black dashed box) is far from the conventional transition frequency of the system, and involves the $|101\rangle$ state and $|010\rangle$ state only, which reflects the $|101\rangle \leftrightarrow |010\rangle$ transition we expected. We can calculate ξ_{drive} with Eq. (4), the results are shown in Fig. 2(b). We observe a driven ZZ interaction ξ_{drive} of $\sim$2 MHz, with the static ZZ interaction negligible. We further calculate ξ_{drive} with varying microwave drive strength, the results are shown in Fig. 2(c), a maximum $\sim$ 3 MHz driven ZZ interaction can be achieved in this process. We note that the proper microwave drive frequency to obtain maximum ξ_{drive} depends on the microwave drive strength Ω_{d} due to the ac-Stark shift induced by the strong microwave drive, the relation of the proper microwave drive frequency and Ω_{d} is also shown in Fig. 2(c).

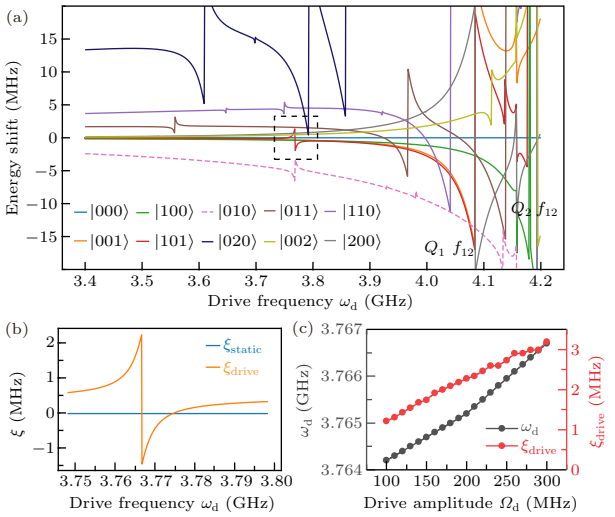


Fig. 2. Driven ZZ interaction calculation. (a) The eigenenergy shift of each eigenstate after introducing microwave drive, with computational states displayed in bold lines. Each eigenstate's energy shift fluctuation reflects a microwave-induced transition starting from this eigenstate. The energy shift fluctuation related to the CZ gate scheme is marked in the dashed box. (b) Static and driven ZZ interaction of the system with microwave drive frequency within the dashed box in panel (a). (c) Driven ZZ interaction versus the microwave drive amplitude (red), and the proper microwave drive frequency to induce maximum driven ZZ interaction versus the microwave drive amplitude (black).

We then move on to simulate the system evolution with microwave drive in time domain. The simulation is performed with QuTiP[29,30] by numerically calculating the Schrödinger equation. The evolution of the system is dominated by the circuit Hamiltonian (1) and the microwave drive Hamiltonian (2). The system is initialized at the $|101\rangle$ state, and we monitor the population of states $|101\rangle$ and $|010\rangle$ during the evolution with varying microwave drive frequency. The results are shown in Figs. 3(a) and 3(b). We observe a population exchange between states $|101\rangle$ and $|010\rangle$ with the Chevron pattern, which indicates a coherent exchange between these states. We note that the CZ gate can only be triggered by a microwave drive with quite precise frequency (within 10 MHz), not to mention stray microwave crosstalk with much less amplitude. So the microwave crosstalk is only of importance when two adjacent couplers require very close microwave drive frequencies (several MHz), which further simplifies frequency management in an extended system. We further examine the influence of microwave drive on other computational states. As plotted in Fig. 3(c), the system starts from $(1/2)(|000\rangle + |001\rangle + |100\rangle + |101\rangle)$ and we monitor the population of all states within two excitations during the evolution. We observe minor fluctuations in populations of states $|100\rangle$ and $|001\rangle$, which are possibly related to this off-resonant

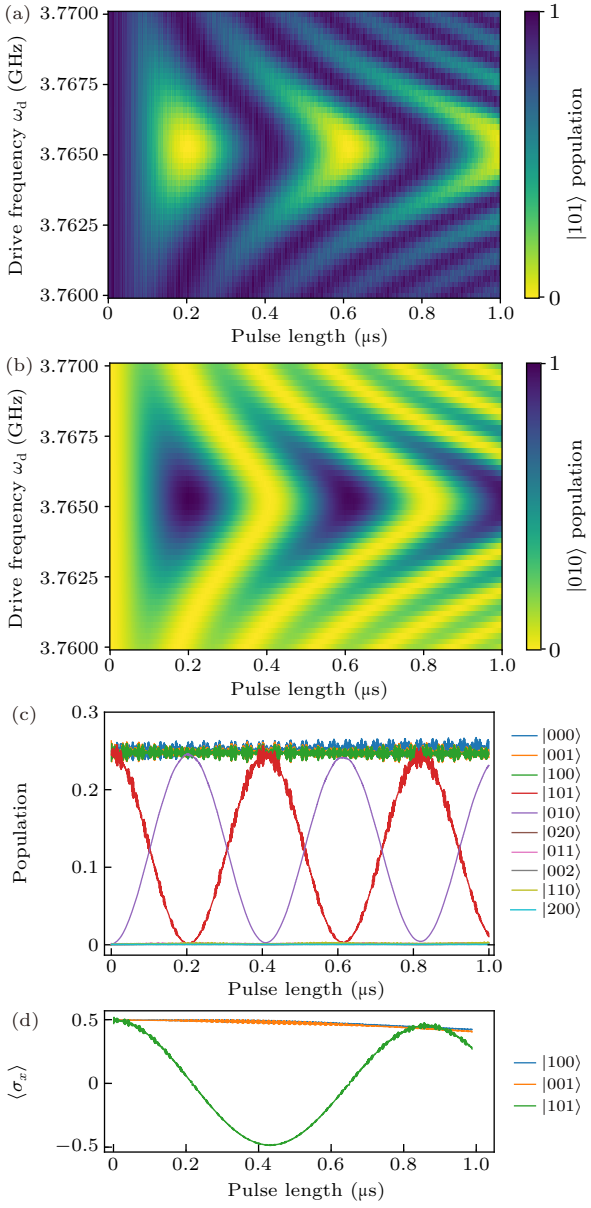


Fig. 3. Time evolution of the system with microwave drive. The population of the $|101\rangle$ state (a) and the $|010\rangle$ state (b) during the evolution with varying microwave drive frequency. (c) The population of each eigenstate and (d) the phase of each computational state during the evolution starting from $(1/2)(|000\rangle + |001\rangle + |100\rangle + |101\rangle)$.

microwave drive. The system's $|101\rangle$ state accumulates phase during the evolution, which enables a CZ gate, as shown in Fig. 3(d). States $|100\rangle$ and $|001\rangle$ also acquire additional phase during the evolution, as a consequence of the minor fluctuations in populations mentioned above, yet this problem can be easily compensated with single-qubit Z rotations.

With CZ gate length and drive frequency extracted from Fig. 3, we further assess the quality of the gate with numerical calculation. Gates with various microwave drive strengths Ω_d (which also leads to various gate lengths) are calibrated according to Fig. 3(c), and their performances are compared in Fig. 4(a). The pink line represents the fidelity of CZ gates with varying microwave drive strength Ω_d, a maximum theoretical gate fidelity above 99.9% can be achieved with $\Omega_\mathrm{d} = 100$ MHz, yet the fidelity declines with increasing microwave drive strength due to spurious effects accompanied by strong microwave drive. The black dashed line is the estimated decoherence error calculated with gate length and parameter $T_1 = T_2^* = 200$ μs for all qubits and the coupler.[31] The maximum gate fidelity would not be available in practice due to decoherence error, which can be alleviated by introducing shorter microwave drive with pulse-shaping technique.[32–35] We further investigate the leakage to non-computational states during the gate. As shown in Fig. 4(b), most of the total gate error (black) can be allocated to leakage error (brown), the remaining gate error is related to phase error due to imperfect gate calibration. As the coupler acquires population during the gate process, we additionally calculate the leakage to the $|010\rangle$ state (yellow). The result shows that this leakage channel contributes little to the total leakage error.

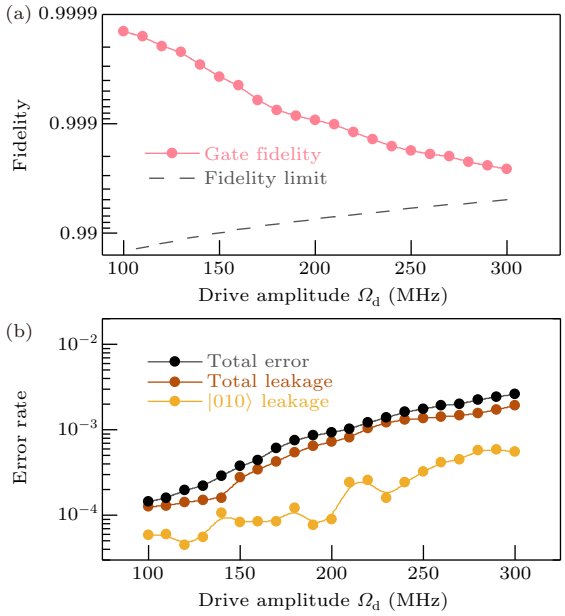


Fig. 4. Gate quality and error analysis of the CZ gate scheme. (a) The calculated gate fidelity (pink) and the fidelity limited by decoherence error (gray) versus the microwave drive amplitude. (b) The total gate error (black), total leakage error (brown), and leakage to $|010\rangle$ (yellow) versus the microwave drive amplitude.

In conclusion, we propose a novel type of all-microwave two-qubit gate with fixed-frequency qubits based on the coupler structure. This gate enables a CZ gate between data qubits with transverse and longitudinal coupling suppressed by the coupler. We numerically calculate the effective drive-induced ZZ interaction during the gate process and simulate the system evolution in time domain. We characterize the gate performance, with theoretical gate fidelity up to 99.9%, and attribute most gate infidelity to the leakage error. The gate performance will further benefit from stronger microwave drive with optimized pulse shape. This gate scheme is activated with a microwave drive applied to the coupler with frequency far away from any direct transition of the system, offering a new solution to the frequency-crowding problems in large-scale quantum computing.

Acknowledgments

Project supported by the Key-Area Research and Development Program of Guangdong Province, China (Grant No. 2020B0303030002), the Strategic Priority Research Program of the Chinese Academy of Sciences (Grant No. XDB0670000), and the National Key Research and Development Program of China (Grant No. 2023YFB4404904).

References

[1] DiVincenzo D P 2000 *Fortschritte der Physik* **48** 771
[2] Krantz P, Kjaergaard M, Yan F, Orlando T P, Gustavsson S and Oliver W D 2019 *Appl. Phys. Rev.* **6** 021318
[3] Kwon S, Tomonaga A, Lakshmi Bhai G, Devitt S J and Tsai J S 2021 *J. Appl. Phys.* **129** 041102
[4] Arute F, Arya K, Babbush R, *et al.* 2019 *Nature* **574** 505
[5] Cao S, Wu B, Chen F, Gong M, Wu Y, Ye Y, Zha C, Qian H, Ying C, Guo S, Zhu Q, Huang H L, Zhao Y, Li S, Wang S, Yu J, Fan D, Wu D, Su H, Deng H, Rong H, Li Y, Zhang K, Chung T H, Liang F, Lin J, Xu Y, Sun L, Guo C, Li N, Huo Y H, Peng C Z, Lu C Y, Yuan X, Zhu X and Pan J W 2023 *Nature* **619** 738
[6] Song C, Xu K, Li H, Zhang Y R, Zhang X, Liu W, Guo Q, Wang Z, Ren W, Hao J, Feng H, Fan H, Zheng D, Wang D W, Wang H and Zhu S Y 2019 *Science* **365** 574
[7] Krinner S, Lacroix N, Remm A, Di Paolo A, Genois E, Leroux C, Hellings C, Lazar S, Swiadek F, Herrmann J, Norris G J, Andersen C K, Müller M, Blais A, Eichler C and Wallraff A 2022 *Nature* **605** 669
[8] Bravyi S, Dial O, Gambetta J M, Gil D and Nazario Z 2022 *J. Appl. Phys.* **132** 160902
[9] Reagor M, Osborn C B, Tezak N, *et al.* 2018 *Science Advances* **4** eaao3603
[10] Rigetti C and Devoret M 2010 *Phys. Rev. B* **81** 134507
[11] Chow J M, Córcoles A D, Gambetta J M, Rigetti C, Johnson B R, Smolin J A, Rozen J R, Keefe G A, Rothwell M B, Ketchen M B and Steffen M 2011 *Phys. Rev. Lett.* **107** 080502
[12] Mitchell B K, Naik R K, Morvan A, Hashim A, Kreikebaum J M, Marinelli B, Lavrijsen W, Nowrouzi K, Santiago D I and Siddiqi I 2021 *Phys. Rev. Lett.* **127** 200502
[13] Noguchi A, Osada A, Masuda S, Kono S, Heya K, Wolski S P, Takahashi H, Sugiyama T, Lachance-Quirion D and Nakamura Y 2020 *Phys. Rev. A* **102** 062408
[14] Sete E A, Didier N, Chen A Q, Kulshreshtha S, Manenti R and Poletto S 2021 *Phys. Rev. Appl.* **16** 024050
[15] Krinner S, Kurpiers P, Royer B, Magnard P, Tsitsilin I, Besse J C, Remm A, Blais A and Wallraff A 2020 *Phys. Rev. Appl.* **14** 044039
[16] Shirai S, Okubo Y, Matsuura K, Osada A, Nakamura Y and Noguchi A 2023 *Phys. Rev. Lett.* **130** 260601

[17] Setiawan F, Groszkowski P and Clerk A A 2023 *Phys. Rev. Appl.* **19** 034071

[18] Li S, Fan D, Gong M, Ye Y, Chen X, Wu Y, Guan H, Deng H, Rong H, Huang H, *L et al*. 2022 *Chin. Phys. Lett.* **39** 030302

[19] Paik H, Mezzacapo A, Sandberg M, McClure D T, Abdo B, Córcoles A D, Dial O, Bogorin D F, Plourde B L T, Steffen M, Cross A W, Gambetta J M and Chow J M 2016 *Phys. Rev. Lett.* **117** 250502

[20] Yan F, Krantz P, Sung Y, Kjaergaard M, Campbell D L, Orlando T P, Gustavsson S and Oliver W D 2018 *Phys. Rev. Applied* **10** 054062

[21] Xu Y, Chu J, Yuan J, Qiu J, Zhou Y, Zhang L, Tan X, Yu Y, Liu S, Li J, *et al*. 2020 *Phys. Rev. Lett.* **125** 240503

[22] Collodo M C, Herrmann J, Lacroix N, Andersen C K, Remm A, Lazar S, Besse J C, Walter T, Wallraff A and Eichler C 2020 *Phys. Rev. Lett.* **125** 240502

[23] Xu H, Liu W, Li Z, Han J, Zhang J, Linghu K, Li Y, Chen M, Yang Z, Wang J, *et al*. 2021 *Chin. Phys. B* **30** 044212

[24] Ye Y, Cao S, Wu Y, Chen X, Zhu Q, Li S, Chen F, Gong M, Zha C, Huang H L, *et al*. 2021 *Chin. Phys. Lett.* **38** 100301

[25] Anandan J 1992 *Nature* **360** 307

[26] Sjöqvist E 2015 *International Journal of Quantum Chemistry* **115** 1311

[27] Lescanne R, Deléglise S, Albertinale E, Réglade U, Capelle T, Ivanov E, Jacqmin T, Leghtas Z and Flurin E 2020 *Phys. Rev. X* **10** 021038

[28] Paolo A D, Leroux C, Hazard T M, Serniak K, Gustavsson S, Blais A and Oliver W D 2022 arXiv:2204.08098 [quant-ph]

[29] Johansson J R, Nation P D and Nori F 2012 *Computer Physics Communications* **183** 1760

[30] Johansson J, Nation P and Nori F 2013 *Computer Physics Communications* **184** 1234

[31] Li R, Kubo K, Ho Y, Yan Z, Nakamura Y and Goto H 2024 *Phys. Rev. X* **14** 041050

[32] Motzoi F, Gambetta J M, Rebentrost P and Wilhelm F K 2009 *Phys. Rev. Lett.* **103** 110501

[33] Werninghaus M, Egger D J, Roy F, Machnes S, Wilhelm F K and Filipp S 2021 *npj Quantum Information* **7** 14

[34] Schulte-Herbrüggen T, Glaser S J, Dirr G and Helmke U 2010 *Reviews in Mathematical Physics* **22** 597

[35] Caneva T, Calarco T and Montangero S 2011 *Phys. Rev. A* **84** 022326